Historical Subsurface Cooling in the Tropical Pacific and Its Dynamics

FENG JIANG,[a] RICHARD SEAGER,[a] AND MARK A. CANE[a]

[a] *Lamont-Doherty Earth Observatory, Columbia University, Palisades, New York*

(Manuscript received 2 January 2024, in final form 20 July 2024, accepted 7 August 2024)

ABSTRACT: Understanding how the tropical Pacific responds to rising greenhouse gases in recent decades is of paramount importance given its central role in global climate systems. Extensive research has explored the long-term trends of tropical Pacific sea surface temperatures (SSTs) and the overlying atmosphere, yet the historical change in the upper ocean has received far less attention. Here, we present compelling evidence of a prominent subsurface cooling pattern along the thermocline in the central-to-eastern tropical Pacific since 1958. This subsurface cooling has been argued to be contributing to the observed cooling or lack of warming of the equatorial cold tongue SST. We further demonstrate that different mechanisms are responsible for different parts of the subsurface cooling. In the central-to-eastern equatorial Pacific and the southeastern off-equatorial Pacific, where zonal wind stress strengthens, a pronounced subsurface cooling trend emerges just above the thermocline that is closely tied to increased Ekman pumping. In the eastern equatorial Pacific where zonal wind stress weakens, the westward surface current and eastward Equatorial Undercurrent weaken as well, resulting in reduced vertical current shear and increased ocean stability, which suppresses vertical mixing and leads to local cooling. We conclude that the historical subsurface cooling is primarily linked to dynamical adjustments of ocean currents to tropical surface wind stress changes.

KEYWORDS: Atmosphere-ocean interaction; Climate change; Climate variability; Trends

1. Introduction

Global oceans have unequivocally shown a warming trend in recent decades associated with rising concentrations of greenhouse gases (GHGs) (Bindoff et al. 2019; Cheng et al. 2019). Intriguingly, amid this unabated ocean warming, the subsurface ocean in the tropical Pacific, particularly near the thermocline region, exhibited a cooling trend over the past several decades (Barnett et al. 2005; Han et al. 2006; Ju et al. 2022; Levitus et al. 2005; Seager et al. 2022; Yang et al. 2014; Levitus et al. 2005). This thermocline cooling in the tropical Pacific has been argued to be contributing to mitigating the anticipated sea surface temperature (SST) warming in response to GHGs, leading to the observed cooling or lack of warming in the equatorial cold tongue region (Seager et al. 2019, 2022; Yang et al. 2014).

Given the central role of tropical Pacific in the global climate systems, extensive research has been dedicated to exploring the long-term trends of tropical Pacific SST and the overlying atmosphere in response to rising GHGs forcing (Cane et al. 1997; Chung et al. 2019; Clement et al. 1996; Heede and Fedorov 2021; Olonscheck et al. 2020; Seager et al. 2019; Vecchi et al. 2006; Zhang et al. 2010; Watanabe et al. 2021). Nevertheless, no broad consensus has been achieved on the characteristics and the underlying mechanisms for the historical long-term trends. The inherent uncertainty in the observational datasets hinders assessments of the historical changes in the tropical Pacific (Chung et al. 2019; Solomon and Newman 2012; Olonscheck et al. 2020; Coats and Karnauskas 2017). In addition, the governing dynamics for the long-term trends in the tropics in response to rising GHGs forcing are highly debated, with various competing hypotheses having been proposed to explain different SST trend patterns (Lee et al. 2022; Watanabe et al. 2024). Based on atmospheric hydrological and energy balances, it is hypothesized that the eastern Pacific would warm more than the warm pool (i.e., El Niño–like pattern) due to a slowdown of the Walker circulation, which would reduce thermocline tilt and upwelling. The El Niño–like response also could be induced by the stronger latent heat cooling in the warm west than in the cool east or by cloud radiation forcing (Held and Soden 2006; Knutson and Manabe 1995; Meehl and Washington 1996; Vecchi et al. 2006; Vecchi and Soden 2007; Xie et al. 2010). Most state-of-the-art climate models simulate an El Niño–like warming pattern in response to GHGs forcing, which contrasts with the observed lack of warming in the cold tongue region. This discrepancy is often interpreted as strong internal variability, particularly that related to the interdecadal Pacific oscillation (IPO)/Pacific decadal oscillation (PDO), masking the forced response in the observation (Wang et al. 2012; Dong and Zhou 2014; Kosaka and Xie 2013; Hansen et al. 1997; Watanabe et al. 2021; Olonscheck et al. 2020). Other studies have argued that when the dynamical adjustment in the tropical Pacific Ocean is brought into play, a La Niña–like SST trend pattern might be anticipated as enhanced cooling by equatorial upwelling counteracts the surface warming in the cold tongue (Cane et al. 1997; Clement et al. 1996; Seager et al. 2019, 2022). This so-called ocean dynamical thermostat is often argued to be transient and will dissipate once the subsurface waters that upwell warm in response to climate forcing in their subtropical source regions (Heede et al. 2020; Heede and Fedorov 2021). Although Seager et al. (2019, 2022) argued that a shallowing of the tropical Pacific thermocline was the key to the observed lack of warming in the cold tongue, the historical changes in the upper tropical Pacific Ocean circulation and

Denotes content that is immediately available upon publication as open access.

Corresponding author: Feng Jiang, fjiang@ldeo.columbia.edu

DOI: 10.1175/JCLI-D-24-0007.1

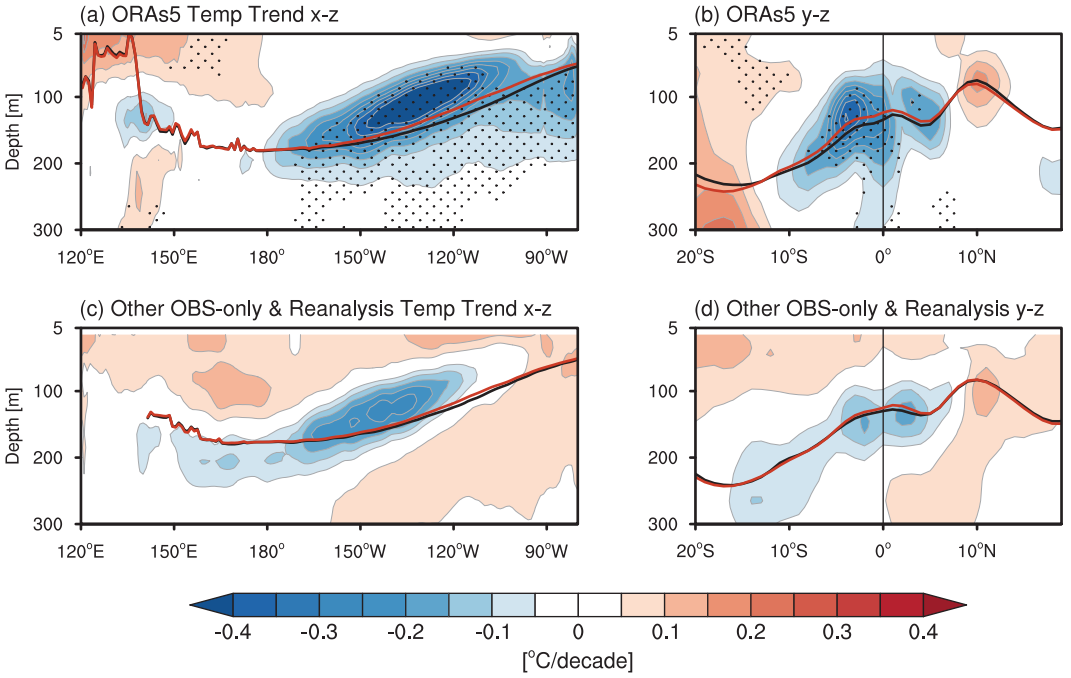

FIG. 1. (a) Meridional mean (5°S–5°N; *x*–*z* plane) and (b) zonal mean (180°–120°W; *y*–*z* plane) subsurface temperature trend (shading; °C per decade) for ORAS5. Black and red lines indicate the thermocline depth in P1 (1958–77) and P2 (2003–22) for ORAS5. Dots in (a) and (b) indicate trend values exceeding the 95% confidence level. (c),(d) As in (a) and (b), but for the composite of other reanalysis and observation-only datasets including SODA2.2.4, EN4, and Ishii.

thermal structure, and what is driving them, have received limited attention.

This subsurface cooling trend in the equatorial tropical Pacific appears to be a robust feature in observations and historical model simulations, despite considerable uncertainty in its longitudinal extent and intensity (Barnett et al. 2005; Han et al. 2006; Ju et al. 2022; Levitus et al. 2005; Luo et al. 2018; Luo and Rothstein 2011; Seager et al. 2022; Yang et al. 2014, 2009; Levitus et al. 2005). Based on coupled climate models subject to increasing carbon dioxide (CO_2), a local minimum of ocean warming appears in the western equatorial thermocline in response to weakened surface wind stress (WS) and the related relaxed thermocline tilt (Vecchi et al. 2006; Vecchi and Soden 2007). Subsequent studies situated this equatorial ocean dynamical feedback process in a broader context of the subtropical cell (STC) system and argued that the slowdown of the STC in response to increasing CO_2 can also significantly contribute to relative cooling of the subsurface compared to the surface in the western equatorial Pacific via weakened meridional and zonal warm advection (Yang et al. 2009; Luo et al. 2018). While model simulations under future warming scenarios or idealized increasing CO_2 experiments generally indicate a forced weakening of the equatorial wind stress, several observation-based studies suggest an intensification of wind stress in the central-to-western Pacific in recent decades (England et al. 2014; Yang et al. 2014). Yang et al. (2014) proposed this contributes to the observed subsurface cooling in the eastern-to-central Pacific (but not the west) over the twentieth century through an accelerated STC and associated upwelling. Nevertheless, it is noteworthy that although the STC displays a general strengthening trend over an extended period from 1900 (Yang et al. 2014), the recent decades with rapidly rising GHGs have not seen such notable trends but rather decadal fluctuations that are closely related to internal variability on interannual-to-decadal time scales (Graffino et al. 2021; Ju et al. 2022; Capotondi and Qiu 2023; McPhaden and Zhang 2004). So far, the underlying mechanisms for the observed subsurface cooling trend prevalent in the central-to-eastern Pacific (Seager et al. 2022), a region known for vigorous ocean–atmosphere interaction processes, remain unclear.

In this study, we focus on how the upper ocean temperatures in the tropical Pacific have changed over the past 6 decades during a rapid increase in GHGs. This paper is structured as follows: Section 2 introduces the data and method employed. Section 3 briefly shows the characteristics of the subsurface cooling in the Pacific based on different sets of reanalysis and observation-only datasets. In sections 4 and 5, we investigate the mechanisms underlying the subsurface cooling, with a particular emphasis on the dynamical adjustments of ocean currents. Section 6 presents the conclusions and discussion.

2. Data and methods

a. Data

To investigate the subsurface temperature change, we utilized the Ocean Reanalysis System-5 (ORAS5) from 1958 to 2022, the latest ocean reanalysis products provided by the

European Centre for Medium-Range Weather Forecasts (ECMWF) (Zuo et al. 2019). The ORAS5 products have a horizontal resolution of 0.25° and 75 vertical levels with a finer 1-m resolution near the surface, which are generated through the Nucleus for European Modelling of the Ocean (NEMO) model driven by atmospheric surface forcing using ERA-40 before 1979, ERA-Interim between 1979 and 2015, and ECMWF NWP since 2015 and constrained by ocean observations (Balmaseda et al. 2015). The subsurface temperature change in another reanalysis dataset, the Simple Ocean Data Assimilation, version 2.2.4 (SODA2.2.4), with horizontal resolutions of 0.25° × 0.4° and 40 vertical layers driven by atmospheric surface forcing using 20CRv2 (Giese and Ray 2011), was also used. Two additional observation-only datasets, version 4 of the Met Office Hadley Centre "EN" series of quality controlled ocean data (EN4) with 1° horizontal resolutions with 42 depth levels (Good et al. 2013) and Ishii data with 1° horizontal resolutions with 42 depth levels (Ishii and Kimoto 2009), were also examined to assess the dependency of the observed subsurface temperature change on products. To maximize overlap in time with ORAS5, we analyzed EN4 data from 1958 to 2022, Ishii data from 1958 to 2012, and SODA2.2.4 data from 1958 to 2008 due to data availability. In addition to temperature T, we obtained zonal current u, meridional current v, surface wind stress τ, and salinity S_a from ORAS5. The vertical velocity w for ORAS5 is calculated from horizontal current velocities u and v based on mass continuity (Vidard et al. 2015).

b. Methods

1) Statistical methods

Anomalies for all variables were calculated as departures from the monthly climatology based on the initial 20 years (1958–77). Statistical significance tests were performed based on the two-tailed Student's t test with an effective number of degrees of freedom $N_{\text{eff}} = N/\{\sum_{i=-(N-1)}^{i=N-1}[1-(i/N)]R(i)^2\}$, where N indicates the sample size and $R(i)$ indicates the autocorrelation of sample series at the lag time of i (Bretherton et al. 1999). The thermocline depth is defined as the depth of 20°C isotherm.

2) Heat budget analysis

The heat budget for each grid point in the subsurface ocean is

$$\frac{\partial T}{\partial t} = -u\frac{\partial T}{\partial x} - v\frac{\partial T}{\partial y} - w\frac{\partial T}{\partial z} + R \equiv \text{ADV} + R. \qquad (1)$$

The residual term R for the subsurface ocean includes diffusive flux, submonthly/subgrid-scale processes, and errors due to data resolution and computation. The advection (ADV) terms can be further decomposed as

$$\begin{aligned}\text{ADV} = {} & \underbrace{-u_a\frac{\partial T}{\partial x}_c}_{\text{UaTc}} \underbrace{-u_c\frac{\partial T}{\partial x}_a}_{\text{UcTa}} \underbrace{-u_a\frac{\partial T}{\partial x}_a}_{\text{UaTa}} \underbrace{-v_a\frac{\partial T}{\partial y}_c}_{\text{VaTc}} \underbrace{-v_c\frac{\partial T}{\partial y}_a}_{\text{VcTa}} \\ & \underbrace{-v_a\frac{\partial T}{\partial y}_a}_{\text{VaTa}} \underbrace{-w_a\frac{\partial T}{\partial z}_c}_{\text{WaTc}} \underbrace{-w_c\frac{\partial T}{\partial z}_a}_{\text{WcTa}} \underbrace{-w_a\frac{\partial T}{\partial z}_a}_{\text{WaTa}}, \end{aligned} \qquad (2)$$

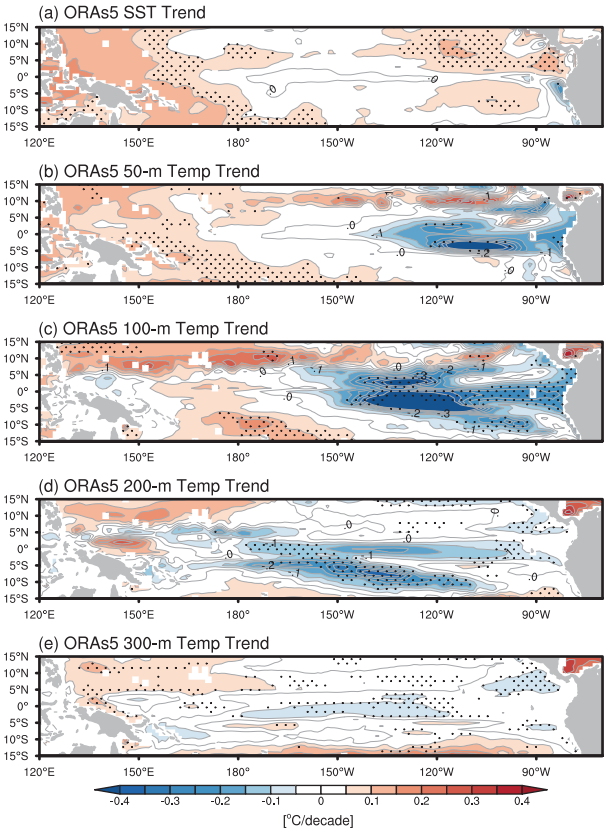

FIG. 2. ORAS5 temperature trends (shading and contour; °C per decade) at (a) 0 m (SST), (b) 50 m, (c) 100 m, (d) 200 m, and (e) 300 m. Dots indicate trend values exceeding the 95% confidence level.

in which a denotes anomaly and c denotes climatology. As such, the advection terms are decomposed into changes in the mean current (UaTc, VaTc, and WaTc), changes in mean temperature gradient (UcTa, VcTa, and WcTa), and nonlinear interactions of anomalies (UaTa, VaTa, and WaTa).

It is challenging to interpret the heat budget of the long-term temperature change. As demonstrated by Alory and Meyers (2009), the temperature change over a long period [the lhs of Eq. (1) averaged over the period] should equal the long-term mean of the heat budget terms [the rhs of Eq. (1) averaged over the period] rather than their changes. Suppose that during a period P1 conditions do not change (e.g., $\overline{\partial T}/\overline{\partial T} \approx 0$ in P1). Therefore, the heat flux [the rhs of Eq. (1)] must sum to zero when averaged over P1, but the individual terms in Eq. (2) will not be zero. One way to understand how changes in individual heat budget terms contribute to the temperature changes is to determine the individual terms in Eq. (2) during such a quasiequilibrium period P1 and then subtract them from the corresponding terms during a period P2 of climate change (He et al. 2022). We note that temperature is little changed during the initial 20 years of the study period (1958–77) and take this to be the reference period P1. We find the average of heat budget terms in the most recent

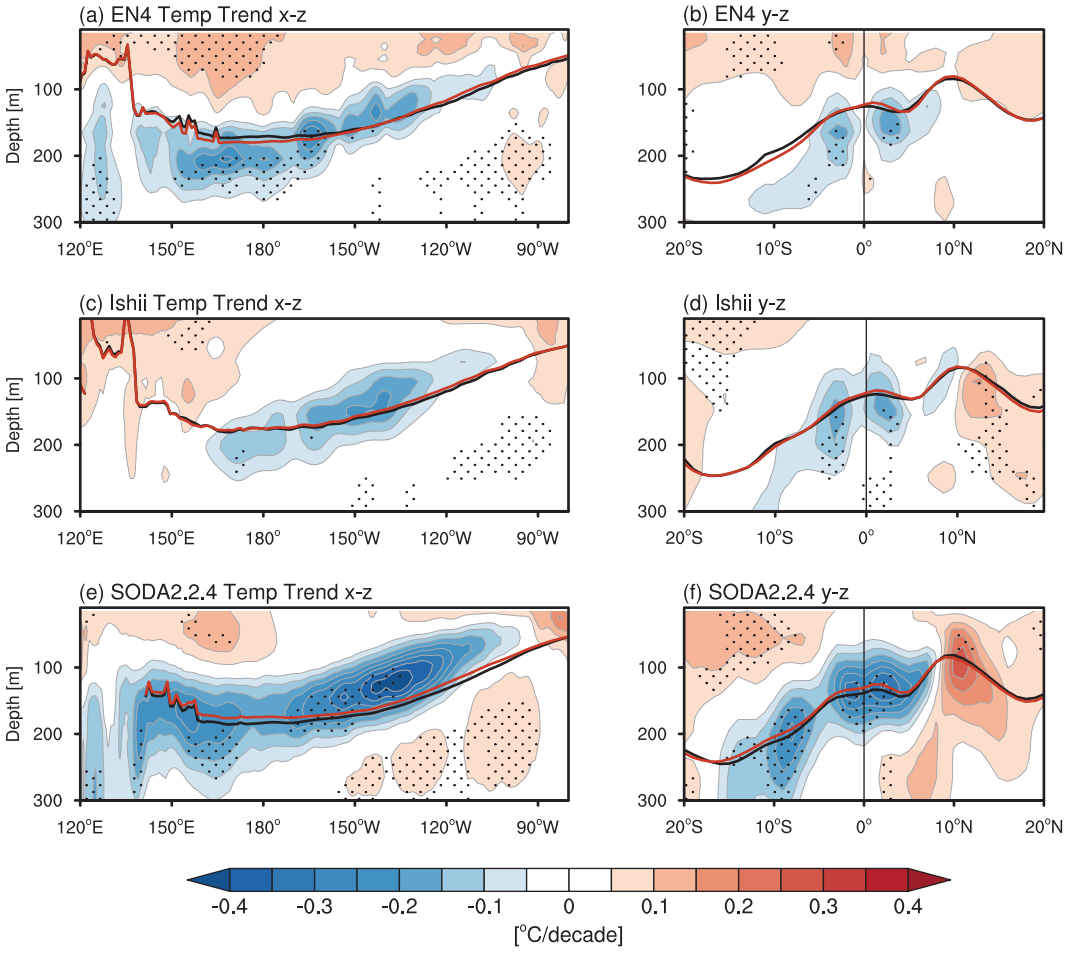

FIG. 3. (a) Meridional mean (5°S–5°N; x–z plane) and (b) zonal mean (180°–120°W; y–z plane) subsurface temperature trend (shading; °C per decade) for EN4. Black and red lines indicate the thermocline depth in P1 and P2 in SODA2.2.4. Dots indicate trend values exceeding the 95% confidence level. (c),(d) As in (a) and (b), but for Ishii. (e),(f) As in (a) and (b), but for SODA2.2.4.

20-yr period (2003–22; P2), when the temperature changed, and subtract the reference state:

$$\overline{\frac{\partial T}{\partial t_{\mathrm{P2}}}} \approx \overline{\frac{\partial T}{\partial t_{\mathrm{P2}}}} - \overline{\frac{\partial T}{\partial t_{\mathrm{P1}}}} = \overline{\mathrm{ADV}}_{\mathrm{P2}} - \overline{\mathrm{ADV}}_{\mathrm{P1}} + \overline{R}_{\mathrm{P2}} - \overline{R}_{\mathrm{P1}}. \quad (3)$$

From Eq. (2),

$$\overline{\frac{\partial T}{\partial t_{\mathrm{P2}}}} \approx [\overline{\mathrm{UaTc}}_{\mathrm{P2}} - \overline{\mathrm{UaTc}}_{\mathrm{P1}}] + \cdots + [\overline{\mathrm{WaTa}}_{\mathrm{P2}} - \overline{\mathrm{WaTa}}_{\mathrm{P1}}] + [\overline{R}_{\mathrm{P2}} - \overline{R}_{\mathrm{P1}}]. \quad (4)$$

The bracketed differences in Eq. (4) are estimates of the contributions of each term to temperature changes, which are used to approximate the long-term trend. Note that the heat budget terms on the lhs of Eqs. (3) and (4) are derived from monthly data (with units of °C per month) and subsequently averaged to obtain the yearly mean (also in °C per month). Then, the difference in the average yearly mean heat budget terms between P1 and P2 is calculated, which retains the units of °C per month.

3) Calculation of the Ekman transport in the tropical region

Following Zebiak and Cane (1987), the Ekman transport $\mathbf{U}_E$ ($\mathrm{m^2\ s^{-1}}$) for the tropical region is formulated by introducing the frictional component of the surface flow as

$$\mathbf{U}_E = \frac{r_s \boldsymbol{\tau} + f(\boldsymbol{\tau} \times \mathbf{k})}{\rho_0 (f^2 + r_s^2)}, \quad (5)$$

where $\boldsymbol{\tau}$ represents the wind stress, r_s represents the surface layer friction coefficient (0.5 $\mathrm{day^{-1}}$), f represents the Coriolis parameter, $\mathbf{k}$ represents the unit vector in the vertical direction, and ρ_0 represents the reference ocean density (1037 kg $\mathrm{m^{-3}}$). The Ekman transport away from the equator approaches $(\boldsymbol{\tau} \times \mathbf{k})/(\rho f)$, consistent with the conventional result based on the Ekman theory. In the near-equatorial region where f approaches 0, the transport approaches $\boldsymbol{\tau}/(\rho r_s)$ and is in the direction of the wind stress.

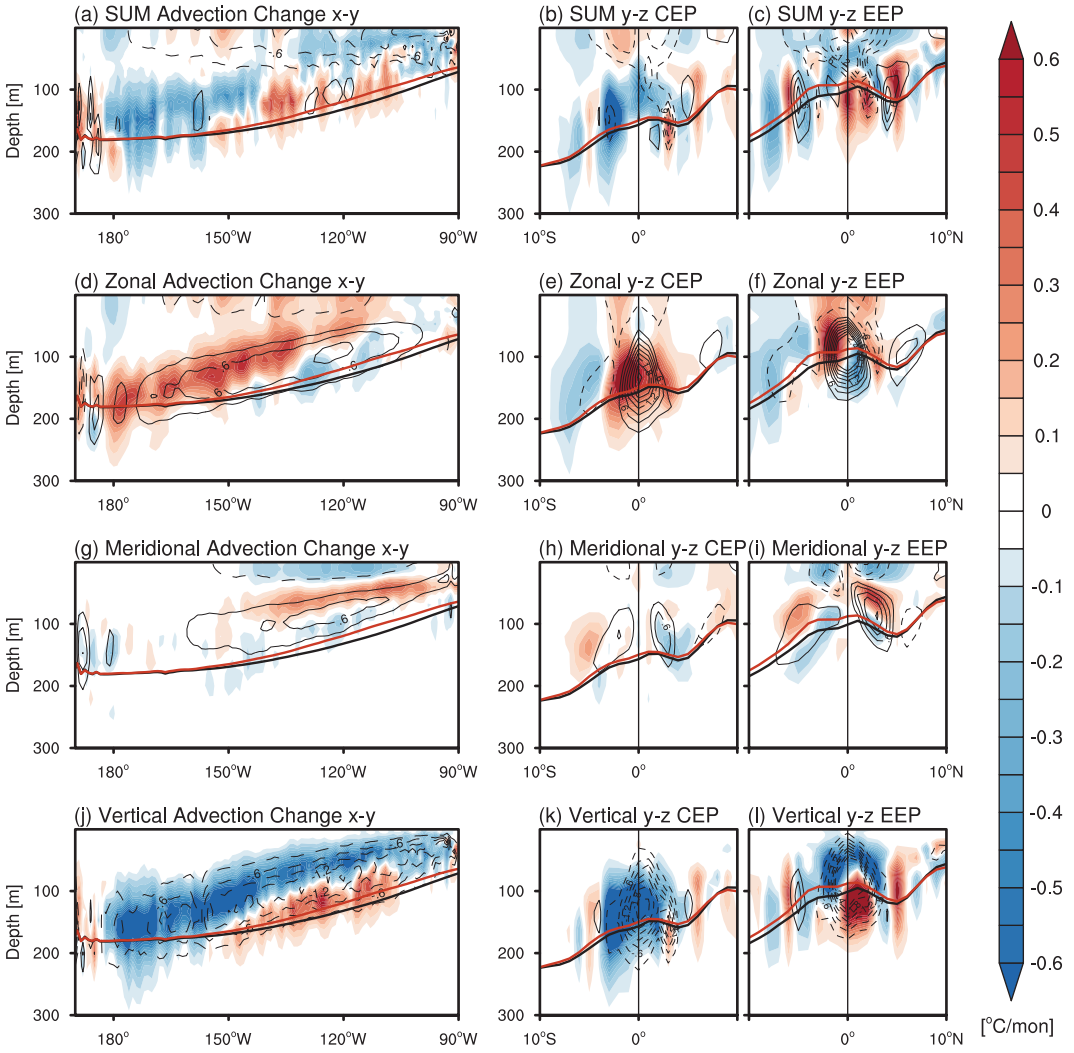

FIG. 4. (a) Meridional mean (5°S–5°N; x–z plane) and zonal mean for (b) the central part of the central-to-eastern Pacific (180°–145°W; y–z plane CEP) and (c) the east part (145°–110°W; y–z plane EEP) of the sum of the climatological ADV terms (contour; °C per month) and the change (P2 minus P1) in the sum of the climatological ADV terms (shading; °C per month). (d)–(f) As in (a)–(c), but for zonal ADV. (g)–(i) As in (a)–(c), but for meridional ADV. (j)–(l) As in (a)–(c), but for vertical ADV. Black and red lines indicate the thermocline depth in P1 and P2 for ORAS5. The positive values indicate warming effects, and the negative values indicate cooling effects.

The friction allows $\mathbf{U}_E$ to be evaluated even as f goes to zero. The Ekman pumping velocity w_E is the divergence of the Ekman transport:

$$w_E = \nabla_H \cdot \mathbf{U}_E. \tag{6}$$

4) CALCULATION OF RICHARDSON NUMBER

The gradient Richardson number (Ri) can be formulated as

$$\mathrm{Ri} = \frac{N^2}{S^2} = \frac{-\frac{g}{\rho_0}\frac{\partial \rho}{\partial z}}{\left(\frac{\partial u}{\partial z}\right)^2 + \left(\frac{\partial v}{\partial z}\right)^2}, \tag{7}$$

where Ri is determined by the Brunt–Väisälä frequency N and vertical current shear S. Here, g is the acceleration of gravity, ρ_0 is the reference ocean density, ρ is the ocean density, u is the zonal current, and v is the meridional current. Utilizing a linear equation of state for seawater, in the top few 100 m, $\partial\rho/\partial z = \alpha\rho_0(\partial T/\partial z) + \beta(\partial S_a/\partial z)$, in which T is the ocean temperature, S_a is the ocean salinity, α is the thermal expansion coefficient ($0.00021°C^{-1}$), and β is the haline contraction coefficient ($0.00074\ \mathrm{psu}^{-1}$).

3. Characteristics of the historical subsurface cooling in the tropical Pacific

Figures 1a, 1b, and 2 show the spatial structure of the linear trend of the upper ocean temperature in the tropical Pacific

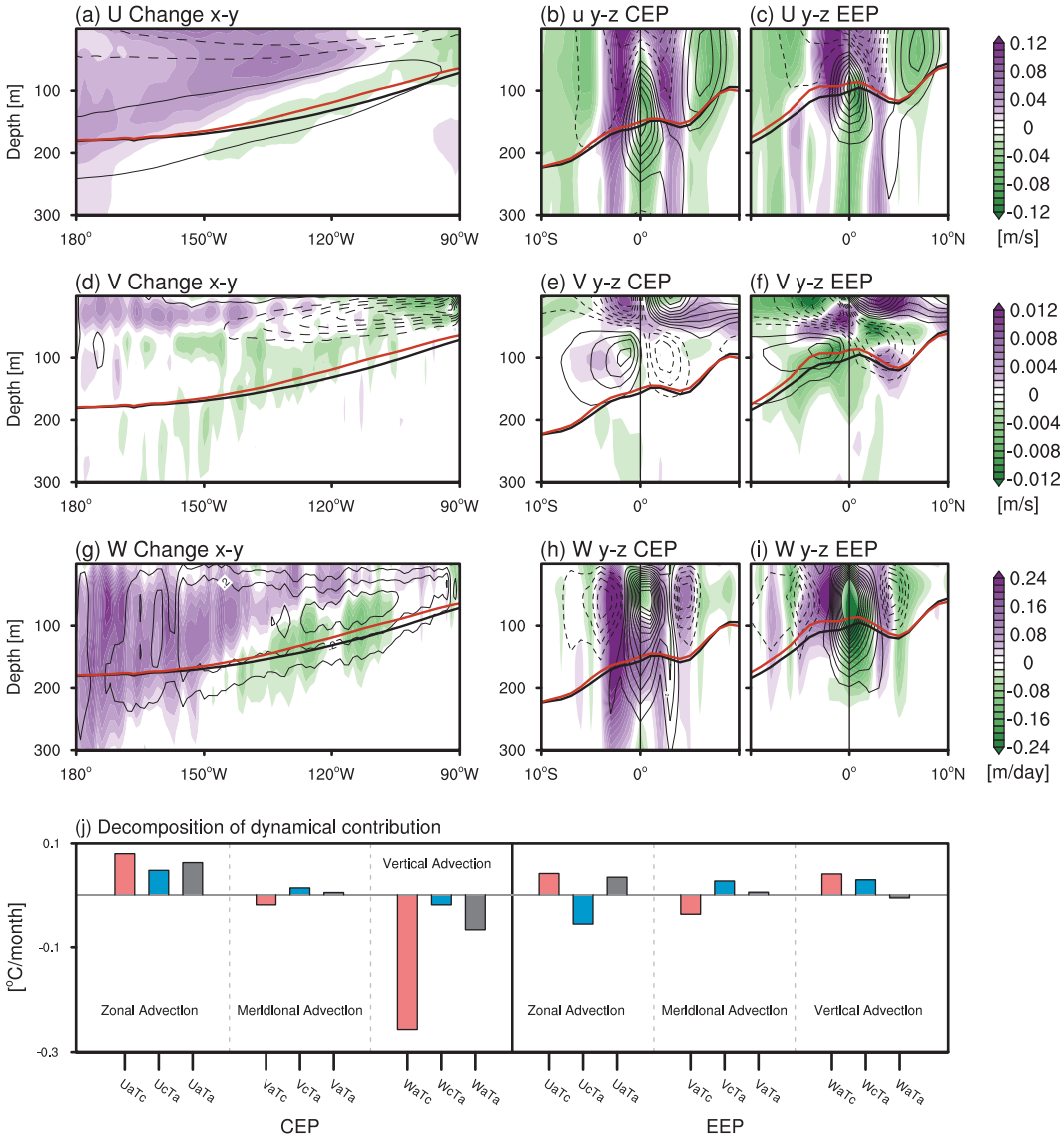

FIG. 5. (a) Meridional mean (5°S–5°N; x–z plane) and zonal mean for (b) CEP (180°–145°W; y–z plane) and (c) EEP (145°–110°W; y–z plane) of the climatological zonal current (contour; m s^{-1}) in P1 and its change (P2 minus P1) (shading; m s^{-1}). (d)–(f) As in (a)–(c), but for meridional current. (g)–(i) As in (a)–(c), but for vertical velocity. Black and red lines indicate the thermocline depth in P1 and P2 for ORAS5. (j) Decomposition of the heat budget terms into zonal current change (UaTc, VaTc, and WaTc), temperature gradient change (UcTa, VcTa, and WcTa), and nonlinear terms (UaTa, VaTa, and WaTa) for the (left) CEP and (right) EEP for the upper portion of the subsurface ocean (70–200 m).

from 1958 to 2022 based on ORAS5. A cooling trend is observed in the subsurface central-to-eastern Pacific, particularly near the thermocline at depths ranging from 50 to 200 m (Fig. 2). The subsurface cooling indicates an enhancing upward tilting of the Pacific thermocline toward the east (Fig. 1a). Extending beyond the equatorial region, the significant cooling trend reaches into the southern off-equatorial region around 10°S and north around 5°N in the eastern Pacific (Figs. 1b and 2). This cooling trend is accompanied by local thermocline shoaling with a maximum of around 10 m in the eastern Pacific by contrasting mean thermocline depths in the most recent and initial 20 years (Figs. 1a,b).

The subsurface cooling trend along the thermocline from 180° to 120°W since 1958 is consistently identified in other reanalysis and observation-only datasets (Figs. 1c,d and 3), despite differences in end years. While the overall spatial structure of the temperature trend is similar across different datasets, there are variations in the exact longitudinal center, meridional extent, and maximum amplitude of the cooling (Fig. 3). In terms of the zonal structure, EN4 and SODA2.2.1 data exhibit an extension of the cooling trend into the western Pacific, whereas ORAS5 and Ishii data show a less pronounced temperature trend in the western Pacific. Regarding

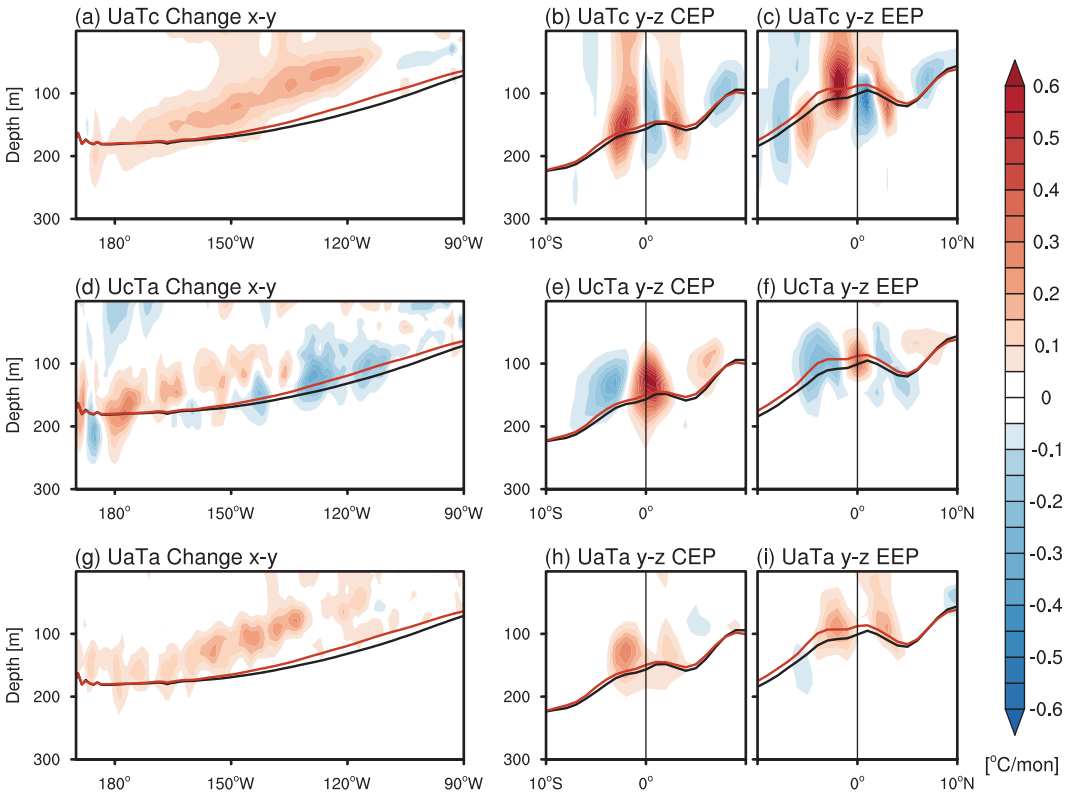

FIG. 6. (a) Meridional mean (5°S–5°N; *x*–*z* plane), (b) zonal mean for CEP (180°–150°W; *y*–*z* plane), and (c) zonal mean for EEP (150°–110°W; *y*–*z* plane) of the change (P2 minus P1) in UaTc (°C per month). (d)–(f) As in (a)–(c), but for UcTa. (g)–(i) As in (a)–(c), but for UaTa. Black and red lines indicate the thermocline depth in P1 for ORAS5.

the meridional structure, the hemispheric asymmetry observed in ORAS5 is less evident in observation-only data (i.e., EN4 and Ishii) but stronger in the other reanalysis data (SODA2.2.1). It is noteworthy that the temperature changes in surface and subsurface regions of the tropical Pacific other than the thermocline exhibit considerable uncertainty across different reanalysis and observational-only datasets, consistent with previous studies (Solomon and Newman 2012). For example, the surface ocean warming in the western equatorial Pacific and the subsurface warming in the southeastern Pacific observed in ORAS5 (Figs. 1a,b) vary among the other three datasets (Fig. 3).

4. Heat budget analysis for the upper tropical Pacific Ocean

The heat budget [Eq. (1)] was first analyzed at each grid point for the reference period P1 (1958–77), when the subsurface temperature is almost constant. The ADV terms for the tropical Pacific subsurface temperature primarily include the zonal advection associated with the South Equatorial Current (SEC) in the surface and the Equatorial Undercurrent (EUC) below, the meridional advection associated with the STCs, the vertical advection related to the upwelling, and the residual. As shown in Figs. 4a–c (contours), there is net advective cooling in the upper portion of the subsurface Pacific including the mixed layer and regions immediately below it. This cooling results from the interplay of westward flow of cold water from the cold tongue to the warm pool in the SEC and the upwelling and off-equatorial divergence of cold tongue water (Figs. 4d,g,j, contours). In the lower portion just above the thermocline, the EUC flows along the thermocline, and the zonal advection and vertical advection largely offset each other, producing little net advective effect. This is consistent with the subsurface flow being along the isotherms. Finally, meridional advection associated with the equatorial portion of the STCs contributes to the subsurface warming in the eastern equatorial Pacific (Figs. 4g–i).

For ~20 years, the observed mean temperature tendency $\overline{\partial T/\partial t}$ is one to two orders of magnitude smaller than the mean of individual heat budget terms in the upper tropical Pacific Ocean. Hence, the dynamical terms must be closely balanced by the residual terms. Previous studies based on model simulations indicate that the advective cooling in the upper equatorial Pacific Ocean can be predominantly counteracted by vertical mixing, which redistributes heat absorbed at the surface to deeper depths (Liu et al. 2005; Ray et al. 2018a,b; Yang et al. 2014). While the monthly resolution of the ORAS5 data does not allow quantitative estimates for vertical mixing, we proceed with the assumption that it is

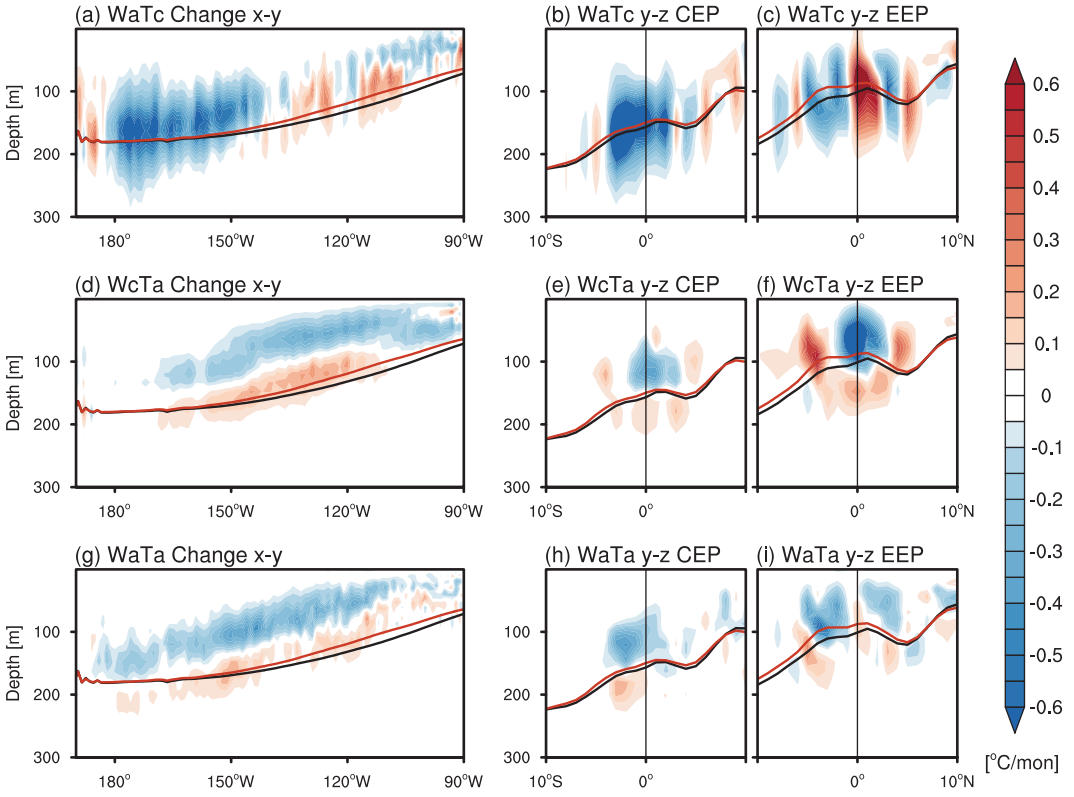

FIG. 7. (a) Meridional mean (5°S–5°N; x–z plane), (b) zonal mean for CEP (180°–150°W; y–z plane), and (c) zonal mean for EEP (150°–110°W; y–z plane) of the change (P2 minus P1) in WaTc (°C per month). (d)–(f) As in (a)–(c), but for WcTa. (g)–(i) As in (a)–(c), but for WaTa. Black and red lines indicate the thermocline depth in P1 for ORAS5.

the primary contributor to the residual terms that balance the advection terms in the subsurface. A later qualitative analysis for the characteristics and possible changes in the vertical mixing lends support to this assumption.

We investigate the changes in heat budget terms that contribute to temperature variations by examining the difference between the most recent and initial 20-yr periods. As shown in Fig. 4, the net effect of the advection terms leads to cooling above the thermocline from 180° to 145°W and cooling in the surface layer and warming near the thermocline from 145° to 110°W (Figs. 4a–c, shadings). We thus divided the central-to-eastern equatorial Pacific into two regions: the central part [central equatorial Pacific (CEP), 5°S–5°N, 180°–145°W] and the east part [eastern equatorial Pacific (EEP), 5°S–5°N, 145°–110°W]. In the CEP, changes in dynamical advection terms effectively account for the subsurface temperature change: The warming effects of strengthened zonal advection (Figs. 4d,e) are overwhelmed by the stronger vertical advective cooling (Fig. 4k). In the EEP, the total effects yield warming near the thermocline region and cooling above (Figs. 4a,c). For the upper part of the EEP, the warming induced by zonal advection is overwhelmed by the cooling from vertical advection, while for the lower part of the EEP, the cooling from zonal advection is overwhelmed by the warming related to vertical advection (Figs. 4f,l). In both CEP and EEP, the influence of the meridional advection is relatively minor (Figs. 4g–i).

The temperature advection terms for the upper portion of the subsurface ocean were further decomposed into changes in mean current, mean temperature gradient, and their nonlinear interaction based on Eq. (2). In the CEP, despite an evident weakening of the EUC in the near-equatorial region, the overall effect of zonal terms yields warming (Figs. 5j and 6), while all vertical terms contribute to cooling, among which the dominant term is WaTc linked to the local strengthening of the upwelling (Figs. 5g–j and 7). In contrast, the role of meridional terms appears relatively minor (Figs. 5d–f,j and 8). In addition to local processes, the STC and the EUC can also be influenced by changes in the western boundary current, thereby affecting the subsurface temperature in the equatorial Pacific (McCreary and Lu 1994; Capotondi et al. 2023).

In the EEP, the contribution from dynamical terms to subsurface cooling is smaller (Fig. 5j). The subsurface cooling induced by the change in zonal temperature gradient (UcTa) counteracts the warming caused by zonal current change (UaTc) and nonlinear terms (UaTa), and the cooling from the meridional current change (VaTc) is offset by the warming induced by the meridional temperature gradient (VcTa). However, the vertical terms (WaTc and WcTa) collectively contribute to warming.

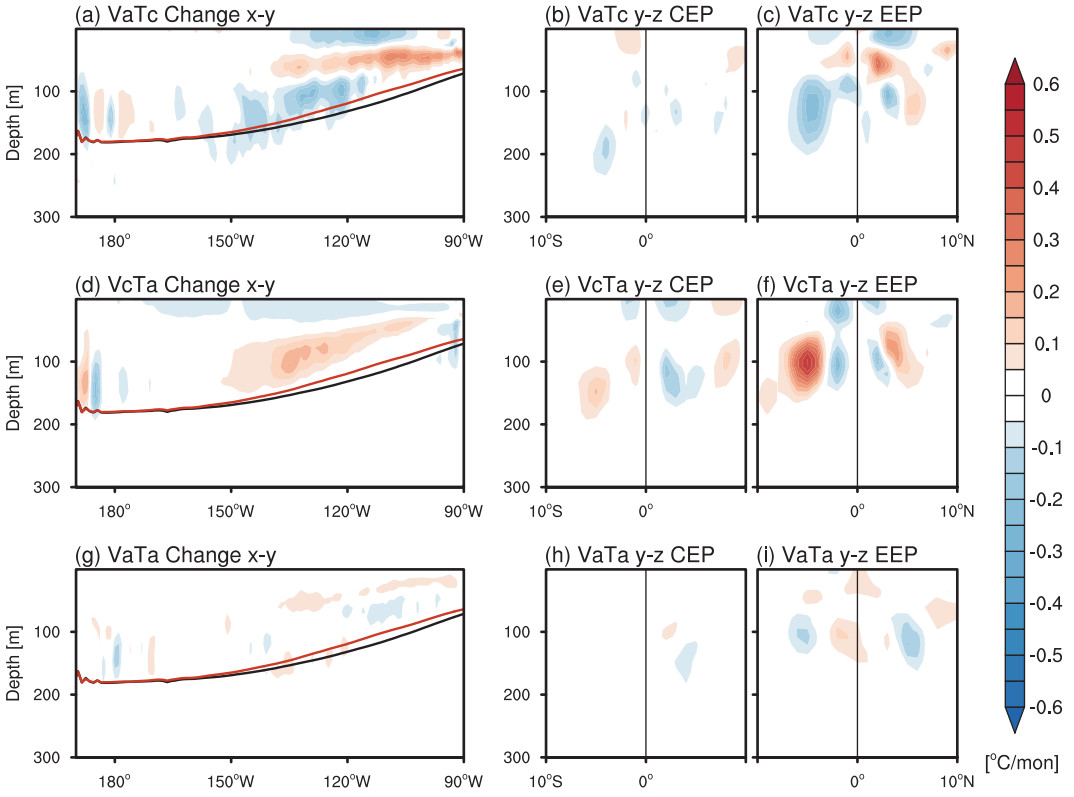

FIG. 8. (a) Meridional mean (5°S–5°N; x–z plane), (b) zonal mean for CEP (180°–150°W; y–z plane W), and (c) zonal mean for EEP (150°–110°W; y–z plane E) of the change (P2 minus P1) in VaTc (°C per month). (d)–(f) As in (a)–(c), but for VcTa. (g)–(i) As in (a)–(c), but for VaTa. Black and red lines indicate the thermocline depth in P1 for ORAS5.

5. Mechanisms for the changes in ocean current and mixing in response to wind stress change

To understand the physical linkage between changes in ocean currents and those in wind stress, we first examine the change in the surface wind stress and estimate the change in the Ekman transport and Ekman pumping velocity based on Eqs. (5) and (6). In the CEP and the off-equatorial region in the southeastern Pacific, there are prominent increases in Ekman upwelling associated with the strengthening of easterly wind stress and increased poleward Ekman transport (Fig. 9). However, in the eastern equatorial Pacific east of 145°W, a weakening of easterly wind stress and decreased poleward Ekman transport lead to a reduction in upwelling locally, consistent with Fig. 5i.

In the subsurface ocean of the eastern equatorial Pacific, the westward SEC and the eastward EUC (Fig. 10a) contribute to a strong vertical current shear above the shallow thermocline, fostering strong mixing despite the large stabilizing vertical temperature gradient (Gregg et al. 1985; Moum et al. 1986). Several modeling studies indicate that the warming effects of the vertical mixing act to balance the net cooling effects of dynamical advection terms and significantly contribute to the large-scale heat budget in the eastern equatorial Pacific (Liu et al. 2005; Ray et al. 2018a; Yang et al. 2014). As the surface wind stress in the eastern equatorial Pacific weakens, both the westward SEC and the eastward EUC weaken (Fig. 10b). Based on a zeroth order model of equatorial circulation, with only the pressure gradient induced by wind stress and vertical momentum diffusion (see details in the appendix), the change in the zonal current in the eastern equatorial Pacific can be qualitatively understood as a response to local wind stress change and local thermocline depth change (Figs. 10b–d).

The weakening of both the westward SEC and eastward EUC results in reduced vertical current shear (Fig. 11a). Based on Eq. (7), the reduced vertical current shear contributes to an increase in Ri, which indicates larger ocean stability. In the NEMO model upon which the ORAS5 product relies (Zuo et al. 2019), changes in ocean stability affect the vertical mixing through a Ri-dependent parameterization of the vertical diffusion (Bernard et al. 2006; Blanke and Delecluse 1993). The parameterized impact of vertical mixing on temperature is expressed as $\partial_z(K_\rho \partial_z T)$, where K_ρ is the vertical diffusivity coefficient. The term K_ρ can be formulated as $K_\rho = (C_k l_k \overline{e}^{1/2})/P_{\mathrm{rl}}$, in which C_k is a constant, $\overline{e}$ is the turbulent kinetic energy (TKE), l_k is the characteristic mixing length that depends on the TKE, and P_{rl} is the Prandtl number, which is 1 for Ri $\leq$ 0.2 or 5Ri for Ri $>$ 0.2. As shown in Fig. 11b, there is a prominent increase in Ri during P2 compared to P1. The corresponding decrease in K_ρ is indicative of

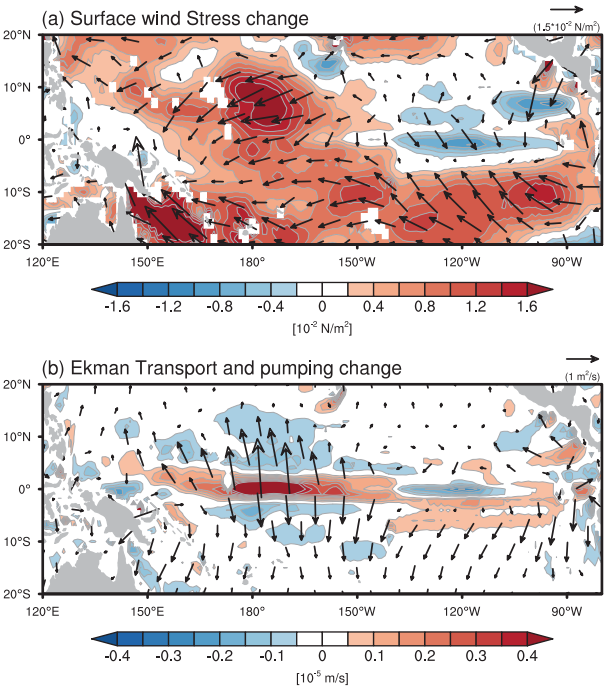

FIG. 9. (a) Changes (P2 minus P1) in the surface WS (vector; N m^{-2}) and its magnitude (shading; N m^{-2}). (b) Changes (P2 minus P1) in the Ekman transport (vector; m^2 s^{-1}) and Ekman pumping velocity (shading; 10^{-5} m s^{-1}).

a reduction in local vertical mixing, and thus, less heat can be redistributed from the surface to deeper depth. We estimate the change in Ri due to current change and stratification change that is related to thermal structure change. Only the contribution of the vertical shear square of the zonal current $(\partial u/\partial z)^2$ is considered since it is much larger than the change in $(\partial v/\partial z)^2$ (not shown). The reduced vertical shear of zonal current (Fig. 11c), rather than the temperature change (Fig. 11d), dominates the change in vertical stability (Fig. 11b) and, we hypothesize, is what leads to suppression of vertical mixing and local subsurface cooling. This wind-driven zonal current change and the related subsurface mixing change offer a feasible explanation for the subsurface cooling above the thermocline in the eastern Pacific (Fig. 1a).

6. Conclusions and discussion

In this study, we investigated the characteristics of the historical subsurface temperature trend in the tropical Pacific and underlying dynamics primarily based on ORAS5 data. We show that a subsurface cooling pattern along the thermocline is evident in the central-to-eastern equatorial Pacific since 1958, which is robust across another reanalysis and observation-only data. We further establish that this cooling is primarily linked to the dynamical adjustment of ocean currents in response to tropical surface wind stress changes through changes in the Ekman pumping and vertical mixing. In the central equatorial Pacific and the southeastern off-equatorial Pacific, where zonal wind stress exhibits a strengthening trend, a pronounced subsurface cooling trend emerges just above the thermocline that is closely tied to the strengthening of Ekman pumping. In the eastern equatorial Pacific where zonal wind stress weakens, the westward surface current and eastward Equatorial Undercurrent weaken as well, resulting in reduced vertical shear and increased ocean stability, which suppresses vertical mixing and leads to local cooling.

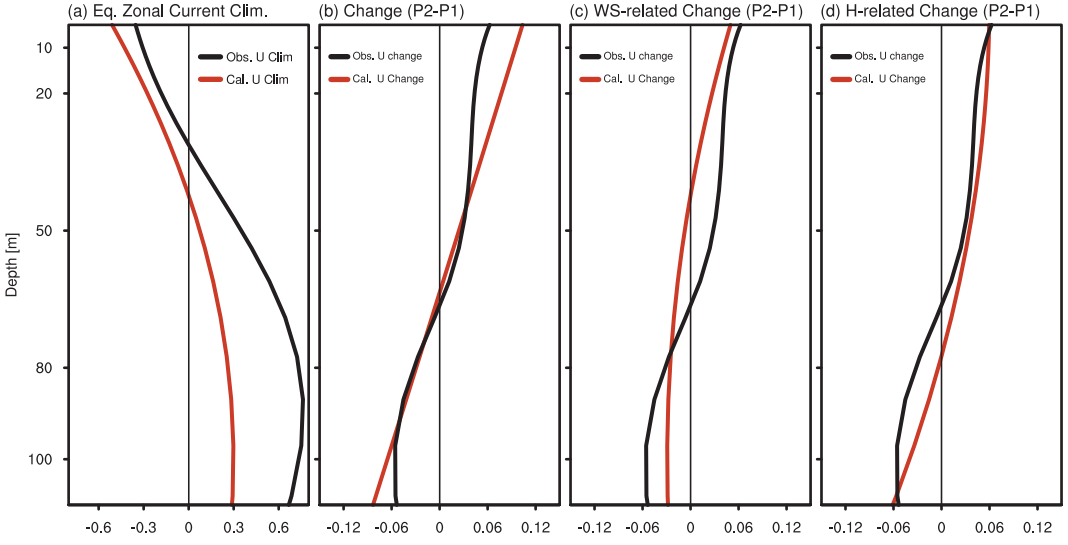

FIG. 10. Vertical profile of (a) the climatology of zonal current in P1 (m s^{-1}) and (b) the change (P2 minus P1) in zonal current (m s^{-1}) averaged over the equatorial eastern Pacific (0°, 145°–110°W). (c),(d) As in (b), but for WS change-related and (d) thermocline depth H change-related zonal current change. Black lines indicate the observed zonal current, and the red lines indicate the calculated zonal current based on the simple momentum balance (see details in the appendix).

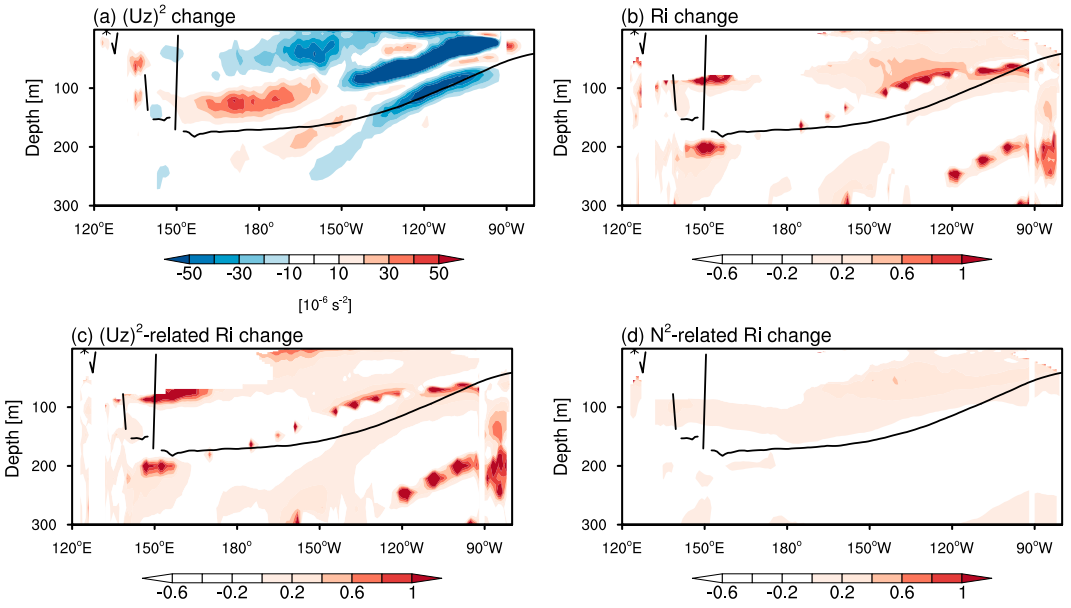

FIG. 11. (a) The change in vertical shear of the zonal current $(\partial u/\partial z)^2$ $[(U_z)^2; 10^{-6}\ s^{-2}]$ averaged over 1°S–1°N. (b) Change in gradient Richardson number Ri (log scale) (P2 minus P1). (b) As in (a), but for change in Ri related to (c) $(U_z)^2$ change and (d) N^2 change. Black line indicates the climatological thermocline depth in P1 for ORAS5.

While we have shown how the changes in the upper tropical Pacific Ocean circulation and thermal structure can be explained as a response to the changes in surface wind stress, the wind stress changes respond to changes in SSTs (Seager et al. 2019) that are influenced by the changes in the upper tropical Pacific Ocean. Seager et al. (2019) argued that thermocline cooling and shoaling were keys to explaining the trend toward an enhanced zonal SST gradient across the equatorial Pacific and that the wind response to that was to strengthen the southeast trades and northeast trades over the west Pacific, much as observed. Current evidence strongly suggests that the coupled tropical Pacific atmosphere–upper ocean system has been evolving over the past 6 decades toward a state characterized by upper thermocline cooling, enhanced equatorial SST gradient, and strengthened trades. Note that it does not rule out other possibilities beyond the ocean dynamical thermostat mechanism, as surface wind stress can also be influenced by remote forcings. Future work needs to determine whether these trends are a tropical Pacific response to anthropogenic effects, such as rising GHGs (Lee et al. 2022), ozone depletion (Hartmann 2022), and nonmonotonic aerosol emissions (Hwang et al. 2024; Takahashi and Watanabe 2016), or whether they come from internal multidecadal variability (Capotondi et al. 2023) or are themselves responding to changes elsewhere such as over the Southern Ocean and southeast Pacific (Dong et al. 2022; Kang et al. 2023).

Last, it is important to acknowledge that although a consistent cooling trend is identified across various ocean reanalysis and observational-only datasets, further efforts are necessary to narrow down the uncertainty surrounding this cooling feature and its underlying mechanisms. As extensively discussed in previous studies (Chung et al. 2019; Solomon and Newman 2012; Olonscheck et al. 2020; Coats and Karnauskas 2017; McGregor et al. 2012; Wittenberg 2004), one should be cautious when analyzing and interpreting the long-term trends in the observation given various issues related to the data quality. This is particularly relevant for ocean data, which are often poorly observed in earlier periods, leading to observations that may be insufficient for accurately determining oceanic diagnostic quantities. The ocean reanalysis data derived from ocean model outputs are driven by presumably more reliable atmospheric data as boundary conditions and constrained by in situ information, but inevitably suffer from the uncertainty in the atmospheric forcing data. For example, the ocean reanalysis ORAS5 uses different generations of atmospheric reanalysis datasets as boundary conditions across time, thereby introducing potential errors related to atmospheric reanalysis uncertainties, including discontinuities in data quality. These inherent data uncertainties may also affect the accuracy of the applied heat budget analyses. Reconciling differences among different observational and analysis datasets poses a continuing challenge for the climate community.

Acknowledgments. This work was supported by the NSF award OCE-2219829. RS received additional support from NSF award AGS-2217618 and DOE award DESC0023333.

Data availability statement. The datasets used to reproduce the results of this paper are located at https://cds.climate.copernicus.eu/cdsapp#!/dataset/reanalysis-oras5?tab=overview (ORAS5 data), http://www.metoffice.gov.uk/hadobs/en4/download-en4-1-1.html (EN4 data), https://rda.ucar.edu/datasets/ds285.3/ (Ishii data), and https://iridl.ldeo.columbia.edu/SOURCES/.CARTON-GIESE/.SODA/.v2p2p4/.temp/ (SODA data).

APPENDIX

A Zeroth-Order Model of the Equatorial Zonal Current

A simplified zonal momentum balance between the zonal pressure gradient force and the vertical friction term in the equatorial eastern Pacific (0°, 145°–110°W, so $f = 0$) can be considered as

$$\nu \frac{\partial}{\partial z}\left[\frac{\partial u(z)}{\partial z}\right] = F_{P_x}, \tag{A1}$$

where u represents the zonal current, ν represents the coefficient of vertical eddy viscosity, and F_{P_x} is the zonal pressure gradient. Here, ν and F_{P_x} are assumed to be depth independent. The term ν is set to be a constant of 3×10^{-3} m^2 s^{-1}, and F_{P_x} can be written in terms of the zonal wind stress τ_x as

$$F_{P_x} = \frac{\tau_x}{\rho_0 H}, \tag{A2}$$

where ρ_0 is the reference ocean density (1037 kg m^{-3}) and H is the thermocline depth. We incorporate the boundary condition:

$$\left.\frac{\partial u(z)}{\partial z}\right|_{z=-H} = 0, \tag{A3}$$

and we assume no net zonal transport in the equatorial plane (0°):

$$\int_{-H}^{0} u(z)dz = 0. \tag{A4}$$

The solution is

$$u(z) = \frac{H\tau_x}{\rho\nu}\left[\frac{1}{2}\left(\frac{z}{H}\right)^2 + \frac{z}{H} + \frac{1}{3}\right]. \tag{A5}$$

Equation (A5) shows a zeroth order model of the zonal current that depends on wind stress and thermocline depth. By using the climatological wind stress and thermocline depth (~100 m) over the near-equatorial eastern Pacific in the first 20 years (P1), we derive the estimated climatological zonal current (red line in Fig. 10a). Then, we can assess the change in the zonal current by calculating the difference between the zonal current in the last 20 years (P2), using the climatological wind stress and thermocline depth (~90 m) in this period, and that in the first 20 years (red line in Fig. 10b). The individual contributions of changes in wind stress and thermocline depth are further elaborated in Figs. 10c and 10d, where each factor is varied independently. The discrepancies between the observed and calculated values (Fig. 10a) may arise from our idealized assumption that ν is constant regardless of the region or depth and also the lack of consideration in the momentum balance of vertical and meridional momentum advection within the broader EUC and STC systems.

REFERENCES

Alory, G., and G. Meyers, 2009: Warming of the upper equatorial Indian Ocean and changes in the heat budget (1960–99). *J. Climate*, **22**, 93–113, https://doi.org/10.1175/2008JCLI2330.1.

Balmaseda, M. A., and Coauthors, 2015: The Ocean Reanalyses Intercomparison Project (ORA-IP). *J. Oper. Oceanogr.*, **8**, s80–s97, https://doi.org/10.1080/1755876X.2015.1022329.

Barnett, T. P., D. W. Pierce, K. M. AchutaRao, P. J. Gleckler, B. D. Santer, J. M. Gregory, and W. M. Washington, 2005: Penetration of human-induced warming into the World's Oceans. *Science*, **309**, 284–287, https://doi.org/10.1126/science.1112418.

Bernard, B., and Coauthors, 2006: Impact of partial steps and momentum advection schemes in a global ocean circulation model at eddy-permitting resolution. *Ocean Dyn.*, **56**, 543–567, https://doi.org/10.1007/s10236-006-0082-1.

Bindoff, N. L., W. W. Cheung, J. Arístegui, V. A. Guinder, R. Hallberg, and N. Hilmi, 2019: Changing ocean marine ecosystems, and dependent communities. *IPCC Special Report on the Ocean and Cryosphere in a Changing Climate*, H.-O. Pörtner et al., Eds., 1st ed. Cambridge University Press, 477–587.

Blanke, B., and P. Delecluse, 1993: Variability of the tropical Atlantic Ocean simulated by a general circulation model with two different mixed-layer physics. *J. Phys. Oceanogr.*, **23**, 1363–1388, https://doi.org/10.1175/1520-0485(1993)023<1363:VOTTAO>2.0.CO;2.

Bretherton, C. S., M. Widmann, V. P. Dymnikov, J. M. Wallace, and I. Bladé, 1999: The effective number of spatial degrees of freedom of a time-varying field. *J. Climate*, **12**, 1990–2009, https://doi.org/10.1175/1520-0442(1999)012<1990:TENOSD>2.0.CO;2.

Cane, M. A., A. C. Clement, A. Kaplan, Y. Kushnir, D. Pozdnyakov, R. Seager, S. E. Zebiak, and R. Murtugudde, 1997: Twentieth-century sea surface temperature trends. *Science*, **275**, 957–960, https://doi.org/10.1126/science.275.5302.957.

Capotondi, A., and B. Qiu, 2023: Decadal variability of the Pacific shallow overturning circulation and the role of local wind forcing. *J. Climate*, **36**, 1001–1015, https://doi.org/10.1175/JCLI-D-22-0408.1.

——, and Coauthors, 2023: Mechanisms of tropical Pacific decadal variability. *Nat. Rev. Earth Environ.*, **4**, 754–769, https://doi.org/10.1038/s43017-023-00486-x.

Cheng, L., J. Abraham, Z. Hausfather, and K. E. Trenberth, 2019: How fast are the oceans warming? *Science*, **363**, 128–129, https://doi.org/10.1126/science.aav7619.

Chung, E.-S., A. Timmermann, B. J. Soden, K.-J. Ha, L. Shi, and V. O. John, 2019: Reconciling opposing Walker circulation trends in observations and model projections. *Nat. Climate Change*, **9**, 405–412, https://doi.org/10.1038/s41558-019-0446-4.

Clement, A. C., R. Seager, M. A. Cane, and S. E. Zebiak, 1996: An ocean dynamical thermostat. *J. Climate*, **9**, 2190–2196, https://doi.org/10.1175/1520-0442(1996)009<2190:AODT>2.0.CO;2.

Coats, S., and K. B. Karnauskas, 2017: Are simulated and observed twentieth century tropical Pacific sea surface temperature trends significant relative to internal variability? *Geophys. Res. Lett.*, **44**, 9928–9937, https://doi.org/10.1002/2017GL074622.

Dong, L., and T. Zhou, 2014: The formation of the recent cooling in the eastern tropical Pacific Ocean and the associated climate impacts: A competition of global warming, IPO, and AMO. *J. Geophys. Res. Atmos.*, **119**, 11 272–11 287, https://doi.org/10.1002/2013JD021395.

Dong, Y., K. C. Armour, D. S. Battisti, and E. Blanchard-Wrigglesworth, 2022: Two-way teleconnections between the Southern Ocean and the tropical Pacific via a dynamic feedback. *J. Climate*, **35**, 6267–6282, https://doi.org/10.1175/JCLI-D-22-0080.1.

England, M. H., and Coauthors, 2014: Recent intensification of wind-driven circulation in the Pacific and the ongoing warming hiatus. *Nat. Climate Change*, **4**, 222–227, https://doi.org/10.1038/nclimate2106.

Giese, B. S., and S. Ray, 2011: El Niño variability in simple ocean data assimilation (SODA), 1871–2008. *J. Geophys. Res.*, **116**, C02024, https://doi.org/10.1029/2010JC006695.

Good, S. A., M. J. Martin, and N. A. Rayner, 2013: EN4: Quality controlled ocean temperature and salinity profiles and monthly objective analyses with uncertainty estimates. *J. Geophys. Res. Oceans*, **118**, 6704–6716, https://doi.org/10.1002/2013JC009067.

Graffino, G., R. Farneti, and F. Kucharski, 2021: Low-frequency variability of the Pacific subtropical cells as reproduced by coupled models and ocean reanalyses. *Climate Dyn.*, **56**, 3231–3254, https://doi.org/10.1007/s00382-021-05639-6.

Gregg, M. C., H. Peters, J. C. Wesson, N. S. Oakey, and T. J. Shay, 1985: Intensive measurements of turbulence and shear in the equatorial undercurrent. *Nature*, **318**, 140–144, https://doi.org/10.1038/318140a0.

Han, W., G. A. Meehl, and A. Hu, 2006: Interpretation of tropical thermocline cooling in the Indian and Pacific oceans during recent decades. *Geophys. Res. Lett.*, **33**, L23615, https://doi.org/10.1029/2006GL027982.

Hansen, J., and Coauthors, 1997: Forcings and chaos in interannual to decadal climate change. *J. Geophys. Res.*, **102**, 25 679–25 720, https://doi.org/10.1029/97JD01495.

Hartmann, D. L., 2022: The Antarctic ozone hole and the pattern effect on climate sensitivity. *Proc. Natl. Acad. Sci. USA*, **119**, e2207889119, https://doi.org/10.1073/pnas.2207889119.

He, C., A. C. Clement, M. A. Cane, L. N. Murphy, J. M. Klavans, and T. M. Fenske, 2022: A North Atlantic warming hole without ocean circulation. *Geophys. Res. Lett.*, **49**, e2022GL100420, https://doi.org/10.1029/2022GL100420.

Heede, U. K., and A. V. Fedorov, 2021: Eastern equatorial Pacific warming delayed by aerosols and thermostat response to CO_2 increase. *Nat. Climate Change*, **11**, 696–703, https://doi.org/10.1038/s41558-021-01101-x.

——, ——, and N. J. Burls, 2020: Time scales and mechanisms for the tropical Pacific response to global warming: A tug of war between the ocean thermostat and weaker walker. *J. Climate*, **33**, 6101–6118, https://doi.org/10.1175/JCLI-D-19-0690.1.

Held, I. M., and B. J. Soden, 2006: Robust responses of the hydrological cycle to global warming. *J. Climate*, **19**, 5686–5699, https://doi.org/10.1175/JCLI3990.1.

Hwang, Y.-T., S.-P. Xie, P.-J. Chen, H.-Y. Tseng, and C. Deser, 2024: Contribution of anthropogenic aerosols to persistent La Niña-like conditions in the early 21st century. *Proc. Natl. Acad. Sci. USA*, **121**, e2315124121, https://doi.org/10.1073/pnas.2315124121.

Ishii, M., and M. Kimoto, 2009: Reevaluation of historical ocean heat content variations with time-varying XBT and MBT depth bias corrections. *J. Oceanogr.*, **65**, 287–299, https://doi.org/10.1007/s10872-009-0027-7.

Ju, W., Y. Zhang, and Y. Du, 2022: Subsurface cooling in the tropical Pacific under a warming climate. *J. Geophys. Res. Oceans*, **127**, e2021JC018225, https://doi.org/10.1029/2021JC018225.

Kang, S. M., P. Ceppi, Y. Yu, and I.-S. Kang, 2023: Recent global climate feedback controlled by Southern Ocean cooling. *Nat. Geosci.*, **16**, 775–780, https://doi.org/10.1038/s41561-023-01256-6.

Knutson, T. R., and S. Manabe, 1995: Time-mean response over the tropical Pacific to increased CO_2 in a coupled ocean-atmosphere model. *J. Climate*, **8**, 2181–2199, https://doi.org/10.1175/1520-0442(1995)008<2181:TMROTT>2.0.CO;2.

Kosaka, Y., and S.-P. Xie, 2013: Recent global-warming hiatus tied to equatorial Pacific surface cooling. *Nature*, **501**, 403–407, https://doi.org/10.1038/nature12534.

Lee, S., M. L'Heureux, A. T. Wittenberg, R. Seager, P. A. O'Gorman, and N. C. Johnson, 2022: On the future zonal contrasts of equatorial Pacific climate: Perspectives from observations, simulations, and theories. *npj Climate Atmos. Sci.*, **5**, 82, https://doi.org/10.1038/s41612-022-00301-2.

Levitus, S., J. Antonov, and T. Boyer, 2005: Warming of the World Ocean, 1955–2003. *Geophys. Res. Lett.*, **32**, L02604, https://doi.org/10.1029/2004GL021592.

Liu, Z., S. Vavrus, F. He, N. Wen, and Y. Zhong, 2005: Rethinking tropical ocean response to global warming: The enhanced equatorial warming. *J. Climate*, **18**, 4684–4700, https://doi.org/10.1175/JCLI3579.1.

Luo, Y., and L. M. Rothstein, 2011: Response of the Pacific Ocean circulation to climate change. *Atmos.–Ocean*, **49**, 235–244, https://doi.org/10.1080/07055900.2011.602325.

——, F. Liu, and J. Lu, 2018: Response of the equatorial Pacific thermocline to climate warming. *Ocean Dyn.*, **68**, 1419–1429, https://doi.org/10.1007/s10236-018-1209-x.

McCreary, J. P., Jr., and P. Lu, 1994: Interaction between the subtropical and equatorial ocean circulations: The subtropical cell. *J. Phys. Oceanogr.*, **24**, 466–497, https://doi.org/10.1175/1520-0485(1994)024<0466:IBTSAE>2.0.CO;2.

McGregor, S., A. Sen Gupta, and M. H. England, 2012: Constraining wind stress products with sea surface height observations and implications for Pacific Ocean sea level trend attribution. *J. Climate*, **25**, 8164–8176, https://doi.org/10.1175/JCLI-D-12-00105.1.

McPhaden, M. J., and D. Zhang, 2004: Pacific Ocean circulation rebounds. *Geophys. Res. Lett.*, **31**, L18301, https://doi.org/10.1029/2004GL020727.

Meehl, G. A., and W. M. Washington, 1996: El Niño-like climate change in a model with increased atmospheric CO_2 concentrations. *Nature*, **382**, 56–60, https://doi.org/10.1038/382056a0.

Moum, J. N., D. R. Caldwell, C. A. Paulson, T. V. Chereskin, and L. A. Regier, 1986: Does ocean turbulence peak at the equator? *J. Phys. Oceanogr.*, **16**, 1991–1994, https://doi.org/10.1175/1520-0485(1986)016<1991:DOTPAT>2.0.CO;2.

Olonscheck, D., M. Rugenstein, and J. Marotzke, 2020: Broad consistency between observed and simulated trends in sea surface temperature patterns. *Geophys. Res. Lett.*, **47**, e2019GL086773, https://doi.org/10.1029/2019GL086773.

Ray, S., A. T. Wittenberg, S. M. Griffies, and F. Zeng, 2018a: Understanding the equatorial Pacific cold tongue time-mean heat budget. Part I: Diagnostic framework. *J. Climate*, **31**, 9965–9985, https://doi.org/10.1175/JCLI-D-18-0152.1.

——, ——, ——, and ——, 2018b: Understanding the equatorial Pacific cold tongue time-mean heat budget. Part II: Evaluation of the GFDL-FLOR coupled GCM. *J. Climate*, **31**, 9987–10 011, https://doi.org/10.1175/JCLI-D-18-0153.1.

Seager, R., M. Cane, N. Henderson, D.-E. Lee, R. Abernathey, and H. Zhang, 2019: Strengthening tropical Pacific zonal sea surface temperature gradient consistent with rising greenhouse

gases. *Nat. Climate Change*, **9**, 517–522, https://doi.org/10.1038/s41558-019-0505-x.

——, N. Henderson, and M. Cane, 2022: Persistent discrepancies between observed and modeled trends in the tropical Pacific Ocean. *J. Climate*, **35**, 4571–4584, https://doi.org/10.1175/JCLI-D-21-0648.1.

Solomon, A., and M. Newman, 2012: Reconciling disparate twentieth-century Indo-Pacific ocean temperature trends in the instrumental record. *Nat. Climate Change*, **2**, 691–699, https://doi.org/10.1038/nclimate1591.

Takahashi, C., and M. Watanabe, 2016: Pacific trade winds accelerated by aerosol forcing over the past two decades. *Nat. Climate Change*, **6**, 768–772, https://doi.org/10.1038/nclimate2996.

Vecchi, G. A., and B. J. Soden, 2007: Global warming and the weakening of the tropical circulation. *J. Climate*, **20**, 4316–4340, https://doi.org/10.1175/JCLI4258.1.

——, ——, A. T. Wittenberg, I. M. Held, A. Leetmaa, and M. J. Harrison, 2006: Weakening of tropical Pacific atmospheric circulation due to anthropogenic forcing. *Nature*, **441**, 73–76, https://doi.org/10.1038/nature04744.

Vidard, A., P.-A. Bouttier, and F. Vigilant, 2015: NEMOTAM: Tangent and adjoint models for the ocean modelling platform NEMO. *Geosci. Model Dev.*, **8**, 1245–1257, https://doi.org/10.5194/gmd-8-1245-2015.

Wang, B., J. Liu, H.-J. Kim, P. J. Webster, and S.-Y. Yim, 2012: Recent change of the global monsoon precipitation (1979–2008). *Climate Dyn.*, **39**, 1123–1135, https://doi.org/10.1007/s00382-011-1266-z.

Watanabe, M., J.-L. Dufresne, Y. Kosaka, T. Mauritsen, and H. Tatebe, 2021: Enhanced warming constrained by past trends in equatorial Pacific sea surface temperature gradient. *Nat. Climate Change*, **11**, 33–37, https://doi.org/10.1038/s41558-020-00933-3.

——, S. M. Kang, M. Collins, Y.-T. Hwang, S. McGregor, and M. F. Stuecker, 2024: Possible shift in controls of the tropical Pacific surface warming pattern. *Nature*, **630**, 315–324, https://doi.org/10.1038/s41586-024-07452-7.

Wittenberg, A. T., 2004: Extended wind stress analyses for ENSO. *J. Climate*, **17**, 2526–2540, https://doi.org/10.1175/1520-0442(2004)017<2526:EWSAFE>2.0.CO;2.

Xie, S.-P., C. Deser, G. A. Vecchi, J. Ma, H. Teng, and A. T. Wittenberg, 2010: Global warming pattern formation: Sea surface temperature and rainfall. *J. Climate*, **23**, 966–986, https://doi.org/10.1175/2009JCLI3329.1.

Yang, C., B. S. Giese, and L. Wu, 2014: Ocean dynamics and tropical Pacific climate change in ocean reanalyses and coupled climate models. *J. Geophys. Res. Oceans*, **119**, 7066–7077, https://doi.org/10.1002/2014JC009979.

Yang, H., F. Wang, and A. Sun, 2009: Understanding the ocean temperature change in global warming: The tropical Pacific. *Tellus*, **61A**, 371–380, https://doi.org/10.1111/j.1600-0870.2009.00390.x.

Zebiak, S. E., and M. A. Cane, 1987: A model El Niño–Southern Oscillation. *Mon. Wea. Rev.*, **115**, 2262–2278, https://doi.org/10.1175/1520-0493(1987)115<2262:AMENO>2.0.CO;2.

Zhang, W., J. Li, and X. Zhao, 2010: Sea surface temperature cooling mode in the Pacific cold tongue. *J. Geophys. Res.*, **115**, C12042, https://doi.org/10.1029/2010JC006501.

Zuo, H., M. A. Balmaseda, S. Tietsche, K. Mogensen, and M. Mayer, 2019: The ECMWF operational ensemble reanalysis–analysis system for ocean and sea ice: A description of the system and assessment. *Ocean Sci.*, **15**, 779–808, https://doi.org/10.5194/os-15-779-2019.